Rapid Communications

Relativistic slingshot: A source for single circularly polarized attosecond x-ray pulses

Jingwei Wang,[1,2,*] Sergei V. Bulanov,[3] Min Chen,[4,2] Bifeng Lei,[5,6] Yuxue Zhang,[5,6] Rishat Zagidullin,[7] Veronika Zorina,[7] Wei Yu,[1] Yuxin Leng,[1] Ruxin Li,[1] Matt Zepf,[5,6] and Sergey G. Rykovanov[7,†]

[1]*State Key Laboratory of High Field Laser Physics, CAS Center for Excellence in Ultra-intense Laser Science, Shanghai Institute of Optics and Fine Mechanics (SIOM), Chinese Academy of Sciences (CAS), Shanghai 201800, China*

[2]*Collaborative Innovation Center of IFSA, Shanghai Jiao Tong University, Shanghai 200240, China*

[3]*Institute of Physics ASCR, v.v.i. (FZU), ELI-Beamlines Project, 182 21 Prague, Czech Republic*

[4]*Key Laboratory for Laser Plasmas (MoE), School of Physics and Astronomy, Shanghai Jiao Tong University, Shanghai 200240, China*

[5]*Helmholtz Institute Jena, Fröbelstieg 3, 07743 Jena, Germany*

[6]*Faculty of Physics and Astronomy, Friedrich-Schiller-Universität Jena, 07743 Jena, Germany*

[7]*Center for Computational and Data-Intensive Science and Engineering, Skolkovo Institute of Science and Technology, Moscow 121205, Russia*

(Received 13 January 2020; revised 14 June 2020; accepted 1 December 2020; published 15 December 2020)

We propose a mechanism to generate a single intense circularly polarized attosecond x-ray pulse from the interaction of a circularly polarized relativistic few-cycle laser pulse with an ultrathin foil at normal incidence. Analytical modeling and particle-in-cell simulation demonstrate that a huge charge-separation field can be produced when all the electrons are displaced from the target by the incident laser, resulting in a high-quality relativistic electron mirror that propagates against the tail of the laser pulse. The latter is efficiently reflected as well as compressed into an attosecond pulse that is also circularly polarized.

DOI: 10.1103/PhysRevE.102.061201

Coherent x-ray radiation is useful for high spatiotemporal resolution investigation of the structure of matter [1–3]. Many applications require light pulses of short wavelength as well as short duration, such as attosecond x-ray pulses (AXP). The table-top source of attosecond x-ray pulses is mainly based on the high-order harmonic generation driven by moderate intensity ($\sim 10^{14}$ W/cm^2) laser pulses in rare gas [4–6]. However, the intensity of AXP from gas harmonics is typically low because of the low efficiency and the limitation of the intensity of the driving laser. On the other hand, intense attosecond x-ray pulses, capable of x-ray pump x-ray probe experiments [7–9], can be realized from the interactions of relativistic intense laser pulses with plasma via surface high-order harmonics generation [10–17] based on the relativistic Doppler effect [18]. In fact, experiments have demonstrated that the relativistic oscillating mirror [19,20] produced on an overdense plasma surface can generate coherent flashes of x-ray radiation with attosecond duration [12–17].

The possibility of generating *circularly* polarized (CP) AXP has been of much recent interest [21–30]. Circularly polarized AXP is particularly useful for investigating chirality-sensitive light-matter interactions, such as dichroism [31,32], magnetization dynamics [33,34], and probing chiral molecules [35]. However, it is generally difficult to generate circularly polarized harmonics or AXP. Even in the moderate intensity region, researchers have not gotten the breakthrough until recently by using two counter-rotating CP laser pulses interacting with gas [22–24]. It is more challenging in the relativistic regime by laser-plasma interactions. This is because at normal incidence, circularly polarized laser light cannot efficiently generate surface plasma oscillations so that no AXP is produced [20]. At oblique incidence, the efficiencies of the s and p components of a circularly polarized driving laser for harmonics generation are different [20,29], resulting in a low-ellipticity AXP. Although it is, in principle, possible to produce circularly polarized AXP from oblique incidence of a suitable elliptically polarized laser on overdense plasma [28,29], in practice such an approach requires very precise matching of the incident angle and the ellipticity of the driving laser. The conversion efficiency is also low.

In this Rapid Communication we propose a method to generate intense isolated and circularly polarized AXP by using the interaction of relativistically intense circularly polarized few-cycle laser pulses with nanometer foils at normal incidence. It is shown that one can effectively utilize the huge longitudinal charge-separation field, produced when all the electrons are separated from the target, to pull the electron sheet back towards the tail of the laser pulse. The reflected field is then compressed resulting in an attosecond pulse with also a circular polarization.

The dynamics of a plasma surface irradiated by normally incident laser pulses with different polarizations are well studied for the case of thick foils [19,20,36–38] (by the case of *thick* foil we mean a scenario in which the incident laser intensity is much lower than that needed to displace all the electrons from the foil). An intuitive way to understand the character of the surface motion is by making an analogy to a forced oscillator. Just like a spring pulled by a harmonic force makes oscillatory motion, so does the plasma surface under

*wangjw@siom.ac.cn
†S.Rykovanov@skoltech.ru

 ©2020 American Physical Society

the action of a linearly polarized laser pulse and the restoring force from the ions. These oscillations lead to the generation of AXP every time when the surface moves towards the laser. It is also now easy to imagine that if the force slowly builds up and then slowly decays, the plasma surface under the action of a circularly polarized laser pulse will slowly follow its envelope. In this case, no AXP will be generated.

The situation becomes drastically different when the foil is thin or in other words when the intensity of the circularly polarized laser is sufficient to completely separate the electrons from the target. The difference stems from the character of the restoring force. When still inside the target the electrons feel the restoring force proportional to the separation distance of the electron layer from the ions, just like the case of a thick foil. But once outside the target the absolute value of the restoring electrostatic force saturates and does not depend on the distance anymore assuming one-dimensional (1D) geometry. One can make the following analogy. The linear restoring potential for the case of a thin foil is similar to the gravity potential on the surface of the Earth. The laser pulse pushes the electrons, building up the potential energy of the electron sheet proportionally to the distance, just like if one would lift a ping-pong ball above the ground. A ball lifted above the surface and released will reach its highest kinetic energy when it comes exactly back to the ground. The same happens to the electron sheet—when the laser pulse goes down, the potential energy stored in the system transforms to the kinetic energy of the electron sheet and it obtains the maximum gamma factor γ when it reaches the ion background. We call this mechanism the *relativistic slingshot*, by which circularly polarized AXP will be efficiently generated.

Throughout the Rapid Communication we work in the relativistic units where normalized time and space are given by $t = \omega_L t'$ and $\vec{x} = (2\pi/\lambda_L)\vec{x}'$, respectively, the normalized density is $n = n'/n_{cr}$ with the critical density $n_{cr} = m\omega_L^2/4\pi e^2$, the normalized field is $\vec{E} = e\vec{E}'/mc\omega_L$, and the normalized laser vector potential is $\vec{a} = e\vec{A}/mc^2$. Here the stressed quantities are given in the CGS units, ω_L is the laser frequency, λ_L is the laser wavelength, c is the speed of light, and $-e$ and m are electron charge and mass, respectively.

Let us first consider the following self-consistent one-dimensional model of thin-foil-laser-pulse interaction. A circularly polarized short laser pulse propagates in the positive x direction and hits the target initially located at $x = 0$. It is convenient to describe the thin foil distribution function as a δ function in both momentum and configuration spaces. The only parameter describing the foil will then be the normalized areal density $\alpha \equiv nl = (n'/n_{cr})(l'\omega_L/c) = 4\pi e^2 n' l'/m\omega_L c$, where l' is the foil thickness. We have developed the physical model in Ref. [39] to the case of a CP field and gotten the following set of self-consistent equations describing the interaction of a δ-like foil with a circularly polarized laser pulse,

$$\frac{dh}{d\xi} = E_x - \epsilon\frac{u_\perp^2}{1+u_\perp^2}, \tag{1}$$

$$\frac{dx}{d\xi} = \frac{1+u_\perp^2-h^2}{2h^2},$$

$$\frac{dy}{d\xi} = \frac{u_y}{h}, \tag{2}$$

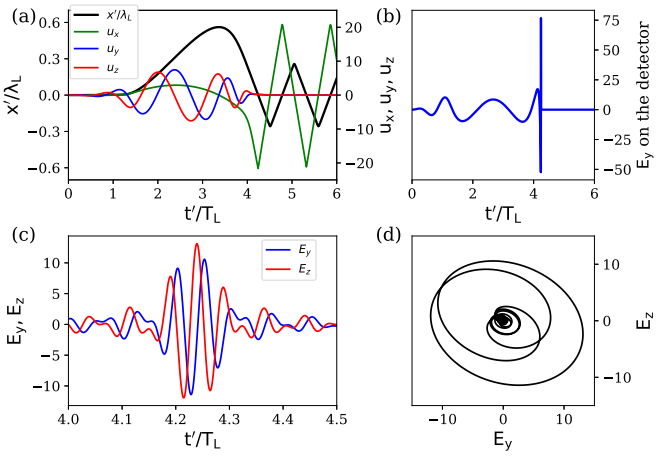

FIG. 1. Results of the numerical solution of the model equations. (a) The longitudinal coordinate x' (black) of the electron layer, the transverse velocity u_y (blue) and u_z (red), and the longitudinal velocity u_x (green) as functions of time. (b) The E_y field radiated by the moving electron layer. (c) The filtered field E_y (blue) and E_z (red) after a bandpass ($7\omega_L \sim 13\omega_L$) filter. (d) The Lissajous curve of the filtered E_y and E_z fields.

$$\frac{dz}{d\xi} = \frac{u_z}{h},$$

$$u_y = a_{y,L} - \epsilon y,$$

$$u_z = a_{z,L} - \epsilon z, \tag{3}$$

where $h = \gamma - u_x$, γ is the relativistic gamma factor, $u_{\{x,y,z\}}$ are the space components of the four-velocity, $u_\perp^2 = u_y^2 + u_z^2$, $\xi = t - x$, $\epsilon = \alpha/2 = 2\pi e^2 n' l'/m\omega_L c$, $a_{y,L}$, and $a_{z,L}$ are the y and z components of laser vector potential $\vec{a}$. Here y and z are conveniently introduced to the 1D model for easier integration, and it is assumed that the electron is initially at $y = 0$ and $z = 0$. $E_x = \epsilon\,\mathrm{sgn}(x)$ is the restoring field arising from the separation of an electron layer from the ion layer. The latter is assumed to be immobile.

In order to fully utilize the strong charge separation fields, it was previously proposed to use the laser pulses with intensity large enough to separate all the electrons of the foil from the ions. Indeed, this has been proved to be useful in accelerating ions or generating relativistic electron mirrors for backscattering. This interaction regime happens when $a_0 \approx \epsilon$ [40], where a_0 is the laser strength parameter defined as the peak amplitude of the laser vector potential $\vec{a}$. For the interaction process proposed in this paper it is also critically important to fully separate the electrons from the ions to build up the electrostatic force, just like one would build up the potential energy in a slingshot. Results of the numerical integration of Eqs. (1)–(4) are presented in Fig. 1.

We use a circularly polarized laser pulse with a $\sin^2$ envelope with a full duration of $4T_L$ and strength parameter $a_0 = 20$ ($\sim 8.5 \times 10^{20}$ W/cm^2 for $\lambda_L = 0.8$ μm). The target has an areal density parameter $\epsilon = 4\pi$, which corresponds to a foil with a thickness of $0.01\lambda_L$ and a density of $400n_{cr}$. Figure 1(a) shows the longitudinal coordinate x', transverse momenta u_y and u_z, and longitudinal momentum u_x all as functions of time. From the behavior of the longitudinal coordinate x' one

can see that first the laser pressure pushes the electron layer effectively away from the ion layer due to the fact that the longitudinal component of the Lorentz force is larger than the constant charge separation field $E_x = \epsilon$. When the laser pulse pressure goes down at some moment of time it reaches the value where it is equal to the electrostatic pressure. This is the moment the slingshot effect takes place. Indeed, the charge separation electrostatic field is equal to 4π and it takes a time less than $0.1T_{\rm L}$ for the electron layer to reach a relativistic velocity whereas swinging backwards. This can be seen on the plot of the u_x of the electron layer as a function of time (green color). During the interaction with a laser pulse the u_x is low, but near the tail of the pulse it rapidly shoots up and reaches the value of about 20. Importantly we note, that when the electron layer swings back, the transverse components of the momentum are not zero. In other words, the electron layer swings back and upshifts the tail of the laser pulse.

To demonstrate this fact more clearly, we have calculated the radiation reflected from the electron layer using the one-dimensional Lienard-Wiechert potential. The radiated electric field in one-dimensional electrodynamics is given by

$$E_{\{y,z\}}(t, x_{\rm d}) = \epsilon u_{\{y,z\}}(t^*)[1 + \beta_x(t^*)]^{-1}, \qquad (4)$$

where $x_{\rm d} < x$ is the position of the detector and $t^* = t + x_{\rm d} - x(t^*)$ is the retarded time. Figure 1(b) demonstrates the E_y field radiated by the electron layer moving with the trajectory given in Fig. 1(a). One can clearly see a single short and intense burst with the amplitude exceeding the amplitude of the incoming laser pulse. Figure 1(c) shows the result of the bandpass filtering of the reflected field from $7\omega_{\rm L}$ to $13\omega_{\rm L}$, exhibiting a clear isolated attosecond pulse with a duration of approximately $0.2T_{\rm L}$. The blue color represents the filtered E_y field, and the red color represents the filtered E_z field. Figure 1(d) shows the Lissajous figure of the filtered E_y and E_z fields, showing that the isolated attosecond pulse is polarized close to circularly with an average ellipticity calculated using the Stokes parameters in the range from $7\omega_{\rm L}$ to $13\omega_{\rm L}$ equal to 0.8. In a word, the self-consistent model clearly predicts the generation of intense isolated attosecond pulses with a polarization very close to circular.

In reality the thin target consists of many electrons interacting with each other, moreover, three-dimensional (3D) effects are not taken into account in the model. To check the predictions of the model, we have conducted series of 1D and 3D particle-in-cell (PIC) simulations using different codes. Results of the 1D PIC simulations using the code PICWIG [37,41] are presented in Fig. 2. The laser pulse and target parameters are taken as the same as in the model calculations presented in Fig. 1. Figure 2(a) demonstrates the dynamics of the foil electron density (color-coded image) as a function of time and space. The motion of the foil qualitatively resembles the sawtooth motion obtained by the model, with a similar amplitude of motion. We present a more detailed comparison between the 1D PIC simulations and the model in the Supplemental Material [42]. In good agreement with the prediction of the model, an isolated intense circularly polarized attosecond pulse is obtained by bandpass filtering the reflected light from $20\omega_{\rm L}$ to $30\omega_{\rm L}$ as seen in Fig. 2(b) which shows the electric-field components E_y and E_z of the obtained attosecond pulse. Figure 2(c) shows the normalized intensity spectrum

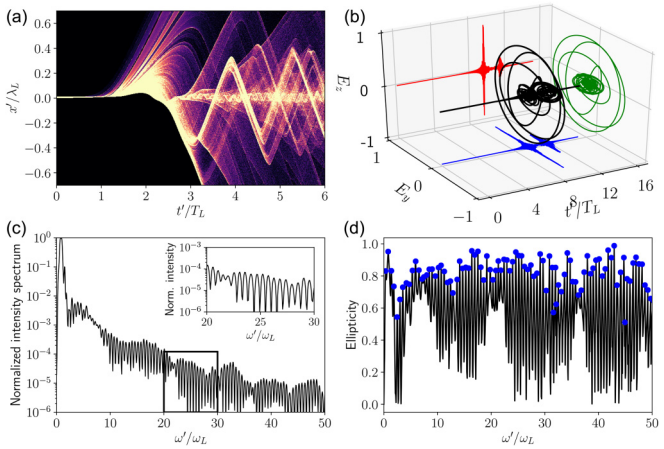

FIG. 2. Results of the 1D PIC simulation. (a) The spatiotemporal evolution of the electron density (color image, densities above $10n_{\rm cr}$ are saturated). (b) Three-dimensional structure of the filtered reflected field showing the circularly polarized AXP (black color). Blue, red, and green curves show projections of the 3D curve on the (t', E_y), (t', Ez), and (Ey, Ez) planes respectively. (c) The spectrum of reflected field. The inlay shows the part of the spectrum remaining after the spectral filtering. (d) The ellipticity values for different frequencies. Blue circles correspond to the peaks of the harmonics whereas the black curve presents ellipticity for all frequencies.

of the reflected light with the inlay demonstrating the part of the spectrum used for obtaining the isolated attosecond pulse. Interestingly one can see the harmonics structure in the spectrum. These harmonics are not multiples of the laser frequency $\omega_{\rm L}$, but multiples of the frequency of the sawtooth oscillations of the foil (the tail of the pulse is reflected by several sawtooth oscillations). The spacing between the harmonics ($\Delta\omega_H \approx 0.55\omega_L$) corresponds exactly to the period of sawtooth oscillations ($\Delta T_{\rm sawtooth} = 1/\Delta\omega_H \approx 1.8T_L$) as seen in Figs. 2(a) and 2(c). This can, in principle, be used in experiments for learning about the dynamics of a thin target irradiated by an intense laser pulse. Finally, Fig. 2(d) presents the ellipticity values for different frequencies. Blue circles correspond to the peaks of the harmonics whereas the black curve presents ellipticity curve for all frequencies. The average ellipticity for all harmonic peaks in the range from 0 to $50\omega_{\rm L}$ is equal to 0.82, whereas in the range from $20\omega_{\rm L}$ to $30\omega_{\rm L}$, used for obtaining the single attosecond pulse, the average ellipticity is equal to 0.86. Hence, the isolated attosecond pulse in Fig. 2(b) has a good level of circular polarization. We note that exact value of the ellipticity may vary depending on the exact parameters of the target and the laser pulse and this will be the subject to the future detailed study.

To check our idea even further we have performed full 3D PIC simulations using the code LAPINE [43–45]. The simulation box is $5\lambda_{\rm L}(\mathbf{x})\times 24\lambda_{\rm L}(\mathbf{y})\times 24\lambda_{\rm L}(\mathbf{z})$ corresponding to grids $5000(\mathbf{x})\times 480(\mathbf{y})\times 480(\mathbf{z})$ with 27 macroparticles per cell. The initial temperature of the plasma is 100 eV. A detailed analysis about how the initial temperature influences the slingshot mechanism is presented in the Supplemental Material [42]. The transverse profile of the laser pulse is Gaussian with a spot size (full width at half maximum) of $12\lambda_{\rm L}$. The other

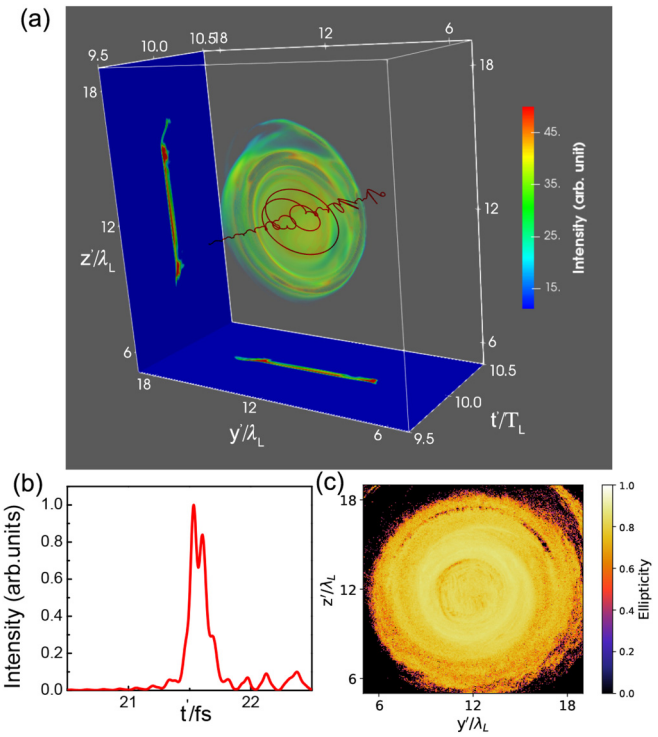

FIG. 3. Results of the 3D PIC simulation. (a) Three-dimensional structure of the intensity of the filtered pulse after a bandpass ($10\omega_L \sim 30\omega_L$) filter. The red line represents the electric field of the pulse along the axis. (b) The temporal shape of the intensity of the filtered pulse showing that the duration of the single attosecond pulse is less than 200 as. (c) The distribution of the average ellipticity of the attosecond pulse in the (y, z) plane showing that the AXP is almost circularly polarized.

parameters of the laser and the target are the same as the 1D case. The result is summarized in Fig. 3. Figure 3(a) demonstrates the 3D structure of the intensity of the attosecond pulse by using the filtered E_y and E_z fields after a bandpass ($10\omega_L \sim 30\omega_L$) filter. It shows that an isolated pulse with a spot size about $6\lambda_L$ is obtained. The duration of the short pulse is less than 200 as, as shown in Fig. 3(b). The peak of the electric field of the generated attosecond pulse is $eE_0/mc\omega_L \simeq 4$. One can then calculate the conversion efficiency from the driving laser pulse to the 200 as pulse is at a level of 10^{-4}. The structure of the electric field of the attosecond pulse along the axis is shown by the red curve in Fig. 3(a), which rotates like the field of a circularly polarized laser pulse. The distribution of the average ellipticity of the selected harmonics ($10\omega_L \sim 30\omega_L$) on the (y, z) plane is presented in Fig. 3(c). One can see that the ellipticity is around 0.9 for the whole pulse, which verifies that the single attosecond pulse is almost circularly polarized. The 3D results agree with the model and the 1D simulation results. It should be mentioned here that the electron layer will deform due to the nonuniform force in the 3D geometry, which introduces different delays for the attosecond pulses from different transverse positions. In order to increase the uniformity one can use a super-Gaussian laser pulse.

Before concluding, we discuss the feasibility and limitations of the slingshot mechanism. First, the areal density or the thickness of the target should be small enough to ensure that the laser intensity can separate all the electrons from the ions. Second, for the slingshot mechanism it is preferable to use a short (few-cycle) pulse. If the pulse is too long, the decay of its intensity is too slow for the electron layer to shoot back vigorously, and the effect will be significantly less. We note that the carrier-envelope phase of the incident short pulse does not play a role because our method relies on the CP laser pulse [42]. Finally, the pulse contrast should be high to avoid over preheating the target so that the possible preplasma length should be still less than the extent of the electron trajectories. The influence of the preplasma length, which is relevant to the initial temperature, is described in the Supplemental Material [42]. Fortunately, the targets and laser systems capable of performing the proposed experiment are readily available in the laboratory [46–51]. For example, laser systems capable of generating circularly polarized laser pulses with intensities around 10^{20} W/cm^2 are available and have already been employed in experiments [50].

In conclusion, we have proposed a simple method to generate circularly polarized AXP, which is promising for the advanced x-ray pump x-ray probe experiments and the study of chirality-sensitive light-matter interactions. The predictions of the analytic theory agree qualitatively with the results of the 1D and 3D PIC simulations. A more systematic parameter investigation including the study of the influence of the plasma surface imperfections (such as roughness and corona) would provide optimal conditions and help for the experimental preparations. The first experimental evidence of the mechanism could be the measurement of the harmonics with the spacing depending on the laser intensity rather than the laser wavelength.

This work was supported by the National Natural Science Foundation of China (NSFC Grants No. 11674341 and No. 11991074), the Helmholtz Association (Young Investigator Group Grant No. VH-NG-1037), the Strategic Priority Research Program of Chinese Academy of Sciences (Grants No. XDA25051100 and No. XDB1603), the Chinese Academy of Sciences President's International Fellowship Initiative (Grant No. 2018VMC0012), and by the Project High Field Initiative (Grant No. CZ.02.1.01/0.0/0.0/15_003/0000449) from the European Regional Development Fund. We gratefully acknowledge the computing time granted by the National Supercomputer Center Tianhe-2 in Guangzhou and Skoltech CDISE supercomputer "Zhores" [52].

[1] D. Attwood, K. Halbach, and K. Kim, Science **228**, 1265 (1985).

[2] R. Neutze, R. Wouts, D. V. D. Spoel, E. Weckert, and J. Hajdu, Nature (London) **406**, 752 (2000).

[3] L. Mino, E. Borfecchia, J. Segura-Ruiz, C. Giannini, G. Martinez-Criado, and C. Lamberti, Rev. Mod. Phys. **90**, 025007 (2018).

[4] P. M. Paul *et al.*, Science **292**, 1689 (2001).

[5] M. Hentschel *et al.*, Nature (London) **414**, 509 (2001).
[6] G. Sansone *et al.*, Science **314**, 443 (2006).
[7] A. Picón *et al.*, Nat. Commun. **7**, 11652 (2016).
[8] T. Pardini, J. Alameda, A. Aquila, S. Boutet, T. Decker, A. E. Gleason, S. Guillet, P. Hamilton, M. Hayes, R. Hill *et al.*, Phys. Rev. Lett. **120**, 265701 (2018).
[9] N. L. Opara *et al.*, Struct. Dyn. **5**, 054303 (2018).
[10] U. Teubner and P. Gibbon, Rev. Mod. Phys. **81**, 445 (2009).
[11] B. Dromey *et al.*, Nat. Phys. **5**, 146 (2009).
[12] Y. Nomura *et al.*, Nat. Phys. **5**, 124 (2009).
[13] P. Heissler *et al.*, Phys. Rev. Lett. **108**, 235003 (2012).
[14] J. A. Wheeler *et al.*, Nat. Photon. **6**, 829 (2012).
[15] M. Yeung *et al.*, Phys. Rev. Lett. **115**, 193903 (2015).
[16] D. Kormin *et al.*, Nat. Commun. **9**, 4992 (2018).
[17] O. Jahn *et al.*, Optica **6**, 280 (2019).
[18] A. Einstein, Ann. Phys. (Leipzig) **322**, 891 (1905).
[19] S. V. Bulanov, N. M. Naumova, and F. Pegoraro, Phys. Plasmas **1**, 745 (1994).
[20] R. Lichters, J. Meyer-ter-Vehn, and A. Pukhov, Phys. Plasmas **3**, 3425 (1996).
[21] E. Allaria, B. Diviacco, C. Callegari, P. Finetti, B. Mahieu, J. Viefhaus, M. Zangrando, G. DeNinno, G. Lambert, E. Ferrari *et al.*, Phys. Rev. X **4**, 041040 (2014).
[22] A. Fleischer, O. Kfir, T. Diskin, P. Sidorenko, and O. Cohen, Nat. Photon. **8**, 543 (2014).
[23] A. Ferré *et al.*, Nat. Photon. **9**, 93 (2015).
[24] D. Hickstein *et al.*, Nat. Photon. **9**, 743 (2015).
[25] G. Lambert *et al.*, Nat. Commun. **6**, 6167 (2015).
[26] A. Depresseux, E. Oliva, J. Gautier, F. Tissandier, G. Lambert, B. Vodungbo, J.-P. Goddet, A. Tafzi, J. Nejdl, M. Kozlova *et al.*, Phys. Rev. Lett. **115**, 083901 (2015).
[27] L. L. Ji *et al.*, Phys. Plasmas **18**, 083104 (2011).
[28] Z.-Y. Chen and A. Pukhov, Nat. Commun. **7**, 12515 (2016).
[29] G. J. Ma, W. Yu, M. Y. Yu, B. F. Shen, and L. Veisz, Opt. Express **24**, 10057 (2016).
[30] K. Hu and H.-C. Wu, Phys. Rev. Lett. **119**, 254801 (2017).
[31] N. Greenfield, Nat. Protoc. **1**, 2876 (2007).
[32] M. Ilchen, N. Douguet, T. Mazza, A. J. Rafipoor, C. Callegari, P. Finetti, O. Plekan, K. C. Prince, A. Demidovich, C. Grazioli *et al.*, Phys. Rev. Lett. **118**, 013002 (2017).
[33] C. Boeglin *et al.*, Nature (London) **465**, 458 (2010).
[34] M. Hennecke, I. Radu, R. Abrudan, T. Kachel, K. Holldack, R. Mitzner, A. Tsukamoto, and S. Eisebitt, Phys. Rev. Lett. **122**, 157202 (2019).
[35] R. Cireasa *et al.*, Nat. Phys. **11**, 654 (2015).
[36] T. Baeva, S. Gordienko, and A. Pukhov, Phys. Rev. E **74**, 046404 (2006).
[37] S. G. Rykovanov *et al.*, New J. Phys. **10**, 025025 (2008).
[38] S. G. Rykovanov *et al.*, New J. Phys. **13**, 023008 (2011).
[39] S. V. Bulanov *et al.*, Phys. Plasmas **20**, 123114 (2013).
[40] A. Macchi, F. Cattani, T. V. Liseykina, and F. Cornolti, Phys. Rev. Lett. **94**, 165003 (2005).
[41] B. Dromey *et al.*, Nat. Phys. **8**, 804 (2012).
[42] See Supplemental Material at https://link.aps.org/supplemental/10.1103/PhysRevE.102.061201 for comparison of the model with 1D PIC simulations, for infuence of the initial plasma temperature, and for infuence of the carrier-envelope phase.
[43] H. Xu *et al.*, Chin. J. Comput. Phys. **19**, 305 (2002).
[44] B. Lei, J. Wang, V. Kharin, M. Zepf, and S. Rykovanov, Phys. Rev. Lett. **120**, 134801 (2018).
[45] J. W. Wang, M. Zepf, and S. G. Rykovanov, Nat. Commun. **10**, 5554 (2019).
[46] D. Kiefer *et al.*, Nat. Commun. **4**, 1763 (2013).
[47] L. Chopineau, A. Leblanc, G. Blaclard, A. Denoeud, M. Thévenet, J.-L. Vay, G. Bonnaud, P. Martin, H. Vincenti, and F. Quéré, Phys. Rev. X **9**, 011050 (2019).
[48] A. Kessel *et al.*, Optica **5**, 434 (2018).
[49] A. K. Geim and K. S. Novoselov, Nat. Mater. **6**, 183 (2007).
[50] C. Scullion *et al.*, Phys. Rev. Lett. **119**, 054801 (2017).
[51] W. J. Ma, I. J. Kim, J. Q. Yu, I. W. Choi, P. K. Singh, H. W. Lee, J. H. Sung, S. K. Lee, C. Lin, Q. Liao *et al.*, Phys. Rev. Lett. **122**, 014803 (2019).
[52] I. Zacharov *et al.*, Open Eng. **9**, 512 (2019).